Geophysical Research Letters

RESEARCH LETTER
10.1029/2019GL083960

Contributions of aerosol-cloud interactions to mid-Piacenzian seasonally sea ice-free Arctic Ocean

Ran Feng[1,2], Bette L. Otto-Bliesner[2], Yangyang Xu[3], Esther Brady[2], Tamara Fletcher[4,5], and Ashley Ballantyne[4]

[1]Department of Geosciences, University of Connecticut, Storrs, CT, USA, [2]Paleo and Polar Climate Division, National Center for Atmospheric Research, Boulder, CO, USA, [3]Department of Atmospheric Sciences, Texas A&M University, College Station, TX, USA, [4]W.A. Franke College of Forestry and Conservation, University of Montana, Missoula, MT, USA, [5]Institute of Applied Ecology, Chinese Academy of Sciences, Shenyang, China

Abstract Forcings and feedbacks controlling the seasonally sea ice-free Arctic Ocean during the mid-Piacenzian Warm period (3.264–3.025 Ma, MPWP), a period when CO_2 level, geography, and topography were similar to present day, remain unclear given that many complex Earth System Models with comparatively higher skills at simulating twentieth century Arctic sea ice tend to produce perennial Arctic sea ice for this period. We demonstrate that explicitly simulating aerosol-cloud interactions and the exclusion of industrial pollutants from model forcing conditions is key to simulating seasonally sea ice-free Arctic Ocean of MPWP. The absence of industrial pollutants leads to fewer and larger cloud droplets over the high-latitude Northern Europe and North Pacific, which allows greater absorption of solar radiation at the surface during the early summer. This enhanced absorption triggers the seasonally runaway sea ice surface albedo feedback that gives rise to September sea ice-free Arctic Ocean and strongly amplified northern high-latitude surface warmth.

Key Points:
- A newer Earth system model simulates September Sea ice-free Arctic Ocean of mid-Piacenzian with realistic boundary and forcing conditions
- The absence of industrial pollutants causes cloud dimming during May and June in the North Pacific and northern Europe
- Early summer warming causes the seasonally runaway ice albedo-surface temperature feedback leading to September Arctic sea ice-free state

Supporting Information:
- Supporting Information S1

Correspondence to:
R. Feng,
ran.feng@uconn.edu

Citation:
Feng, R., Otto-Bliesner, B. L., Xu, Y., Brady, E., Fletcher, T., & Ballantyne, A. (2019). Contributions of aerosol-cloud interactions to mid-Piacenzian seasonally sea ice-free Arctic Ocean. *Geophysical Research Letters*, *46*, 9920–9929. https://doi.org/10.1029/2019GL083960

Received 2 JUN 2019
Accepted 23 JUL 2019
Accepted article online 30 JUL 2019
Published online 26 AUG 2019

1. Introduction

The mid-Piacenzian warm period (MPWP), with global mean surface temperature between 1.9 and 3.6 °C warmer than preindustrial (PI; Haywood & Valdes, 2004; Masson-Delmotte et al., 2013), is widely considered a potential analog for future climate change (Chandler et al., 1994; Haywood & Valdes, 2004) due to similar geography, topography, and CO_2 level as present day and near future (Dowsett et al., 2016; Haywood et al., 2010, 2016). These conditions and the relatively stable MPWP climate, as evidenced by low variability of $\delta^{18}O$ in stacked benthic records (Lisiecki & Raymo, 2005), suggest that the MPWP may provide insights into the equilibrium climate of Earth's future if the world follows a low (Representative Concentration Pathway, RCP 2.6) to medium emission pathway (RCP 4.5; Solomon et al., 2009).

Despite a moderate global mean warming as opposed to PI, MPWP proxy records show strongly amplified warmth across the northern high latitudes and Arctic Ocean relative to the global mean. These records suggest that at multiple sites in the Canadian Arctic Archipelago, annual temperatures were well above freezing (Ballantyne et al., 2010; Csank et al., 2011; Fletcher et al., 2017; Salzmann et al., 2013), with an active fluvial and ecosystems (Rybczynski et al., 2013), and a seasonally sea ice-free Arctic Ocean (Knies et al., 2014; Naafs et al., 2010; Polyak et al., 2010). In contrast, the majority of Earth system models (ESMs) that participated in the Pliocene Model Intercomparison Project phase 1 (PlioMIP1; Haywood et al., 2010) simulate below freezing annual temperatures across the Canadian Arctic Archipelago and perennial Arctic sea ice (Howell, Haywood, Otto-Bliesner, et al., 2016). Half of the ESMs also feature perennial Arctic sea ice condition even including the ones with higher skills at simulating historical Arctic sea ice extent (Howell, Haywood, Otto-Bliesner, et al., 2016). This apparent model-proxy data mismatch cannot be fully resolved by orbital-forcing driven millennial scale climate variability (Feng et al., 2017; Prescott et al., 2014; Salzmann et al., 2013), uncertainty in CO_2 estimates (Feng et al., 2017; Howell, Haywood, Dowsett, et al., 2016; Salzmann et al., 2013), changes in Arctic Ocean gateway configuration (Feng et al., 2017; Otto-Bliesner et al., 2017), or other changes in paleogeography and bathymetry (Hill, 2015; Robinson et al., 2011).

This persistent model-proxy data mismatch has led to the consideration of unconstrained climate forcings, such as tropospheric aerosols. Recently, idealized studies have shown that changes in biogenic emissions

of trace gases and aerosols, and atmospheric dust loading can enhance simulated MPWP warming globally (Unger & Yue, 2014) and in the Arctic (Sagoo & Storelvmo, 2017). The majority of PlioMIP1 models were unable to quantify the effects of aerosol-cloud interactions (ACI). The only model that partially considers ACI is the ModelE of National Aeronautics and Space Administration (Chandler et al., 2013). Simulations of seasonal cycle of MPWP Arctic sea ice by this model is distinctively different from the others (Howell, Haywood, Otto-Bliesner, et al., 2016) in such a way that the winter sea ice is both extensive and thick, yet the model reaches summer (August to September) sea ice-free conditions. Among models using cloud closure schemes derived from observations of relative humidity and temperature profiles of present day (e.g., HadCM3 model, Smith, 1990) or models using prescribed modern background aerosol conditions for cloud formation (e.g. CCSM4 model, Neale, Richter, et al., 2010), simulated clouds are affected by statistics inherent to polluted troposphere and may not be representative for paleoclimate simulations (Kiehl & Shields, 2013; Kump & Pollard, 2008). It is well known that industrial pollutants have substantially altered the aerosol composition and concentration in the atmosphere (Andreae, 2007). Emissions of industrial pollutants may have greatly affected Arctic temperature and sea ice loss (Gagné et al., 2015; Navarro et al., 2016).

Here, by using a 1° horizontal resolution, state-of-the-art coupled ESM, we demonstrate the importance of explicitly simulating ACI in reproducing MPWP seasonally ice-free Arctic Ocean. A greater sensitivity of sea ice response to CO_2 forcing through modifying ice albedo (Howell, Haywood, Dowsett, et al., 2016) or an overall more sensitive ESM to CO_2 forcing (Zheng et al., 2019) has been shown to ameliorate model-proxy data mismatch of Arctic for MPWP. By comparing PlioMIP1 simulations with and without industrial pollutants, we provide an alternative explanation to improvements of PlioMIP simulations between generations of ESMs.

2. Methods

We carried out four experiments using the Community Earth System Model (CESM1.2; Hurrell et al., 2013) branched from an existing PlioMIP1 simulation using the parental model Community Climate System Model version 4 (PlioMIP1-CCSM4; Rosenbloom et al., 2013). CESM1.2 is configured with the atmospheric model CAM5.3, which explicitly simulates indirect effects of aerosols on liquid and ice cloud formation and albedo (Gettelman et al., 2010). For ice cloud, immersion freezing (ice nuclei formed by aerosols) is explicitly treated for cirrus clouds but only implied for mixed phrase clouds (Neale, Gettelman, et al., 2010). The capability of CAM5 models in simulating present-day clouds and aerosol-cloud interactions are evaluated by various studies (Gettelman, 2015; Gettelman et al., 2010; Kay et al., 2012). In general, CAM5 models demonstrate fundamental improvements in simulating cloud and cloud radiative forcing compared to the previous generations (Kay et al., 2012). Across the Arctic region, observed seasonal cycles of total and low clouds show reasonable agreement with observations (Kay et al., 2012; Text S1 in the supporting information).

The four experiments conducted in our study include two atmosphere-ocean-land-sea ice coupled simulations (Plio-Pristine and Plio-Polluted) and two prescribed sea surface temperature (SST) and sea ice simulations. Two aerosol emission scenarios are featured in these simulations, one with preindustrial emissions (Plio-Pristine) and the other with preindustrial emissions plus industrial pollutants of anthropogenic SO_2, sulfate, and organic compounds estimated for the 2000s (Lamarque et al., 2010; Plio-Polluted). Both Plio-Pristine and Plio-Polluted are run for over 300 model years branched from the 500 model year PlioMIP1-CCSM4, which only considers the direct effect (reflecting and scattering, no interactions with clouds) of preindustrial aerosols (Rosenbloom et al., 2013). Quasi-equilibrium is reached towards the end of the runs (Text S1). Climate differences are estimated by differencing Plio-Pristine and Plio-Polluted. Both climatologies and differences are calculated for the final 50 model years.

Two prescribed SST and sea ice simulations are carried out in order to estimate the effective radiative forcings (ERFs) from changing aerosol emissions excluding slow feedbacks from ocean dynamics and sea ice (Myhre et al., 2013). These two simulations use the same atmosphere and land model configuration, and boundary and CO_2 conditions as the coupled CESM1.2 runs. Prescribed SST and sea ice are derived from 50-year averages of PlioMIP1-CCSM4 using the standard method (Hurrell et al., 2008), given that both Plio-Pristine and Plio-Polluted are branched from the PlioMIP1-CCSM4 with the same ocean and sea ice initial state. Further, we exclude feedbacks due to changes in surface snow cover from calculations of ERF

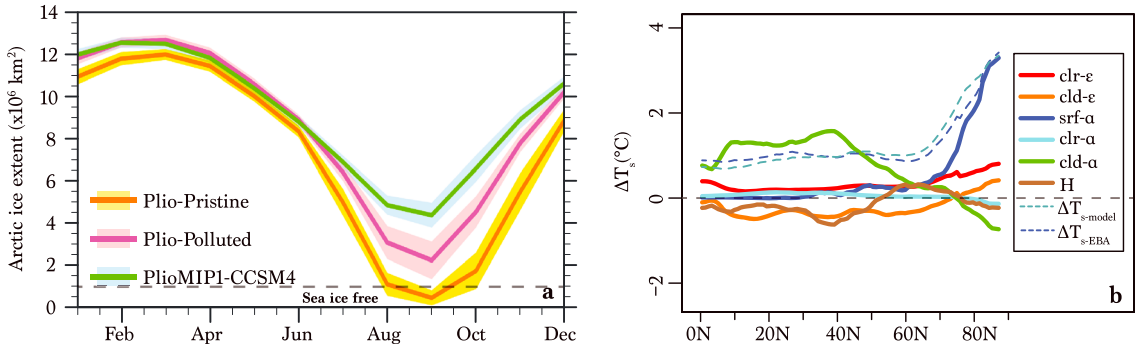

Figure 1. Monthly climatology of simulated Arctic sea ice extent of different experiments, and energy balance analysis of zonal mean annual surface temperature difference (ΔT_s) between Plio-Pristine and Plio-Polluted ($\Delta T_{s\text{-model}}$). (a) Arctic sea ice extent simulated by PlioMIP1-CCSM4, Plio-Pristine, and Plio-Polluted. Shaded areas in (a) are one standard deviations of monthly sea ice extent from 50 model year average. Sea ice-free is defined as Arctic sea ice extent below 10^6 km^2 (Jahn et al., 2016). (b) Model simulated ΔT_s ($\Delta T_{s\text{-model}}$) and ΔT_s due to individual (solid lines) and all radiative components ($\Delta T_{s\text{-EBA}}$). α = shortwave reflection, ε = emissivity; H = heat convergence; srf = surface condition; clr = clear-sky condition; cld = cloudy condition. Gray dashed line in (b) shows the 0° of ΔT_s.

by removing the amount of change in planetary shortwave reflection that is attributable to changes in surface albedo between two prescribed SST and sea ice runs. This adjustment removes 0.1 W/m^2 forcing from global mean and 0.9 W/m^2 forcing from Arctic mean (Text S2). The results are referred to as adjusted effective radiative forcing (aERF). A call to the radiation code prior to computation of aerosols is also included in these experiments to estimate radiative forcing only pertaining to aerosol optical properties without cloud changes, including scattering and absorption, which is termed as direct radiative forcing (F_{dir}; Ghan et al., 2012). The indirect forcing, primarily from ACI, is estimated by subtracting F_{dir} from the aERF.

3. Results

3.1. Simulated Climate Mean States

Global mean annual surface temperature (T_s) of Plio-Pristine is 0.84 °C warmer than Plio-Polluted. This warming is amplified north of 70°N by an additional 1.5 °C with an annual Arctic sea ice reduction of 27% in volume and 14% in coverage. Both Plio-Pristine and Plio-Polluted are warmer than PlioMIP1-CCSM4, attributable to a ~1 °C increase in climate sensitivity of CESM1 per doubling of CO_2 compared to CCSM4 (Meehl et al., 2013). In particular, Plio-Pristine features mean September Arctic sea ice-free conditions. In contrast, Arctic sea ice is perennial in both Plio-Polluted and PlioMIP1-CCSM4 (Figure 1a).

Compared to Plio-Polluted, Plio-Pristine simulates a positive aERF of 1.29 W/m^2, which primarily arises from changes in ACI (Table 1). aERF is only 0.75 W/m^2 across the Arctic (north of 70°N) despite the amplified warming and strong response of sea ice. The global mean aERF estimated here is slightly higher than the 1.1 W/m^2 estimated with present-day SSTs and sea ice cover using the same model (Gettelman et al., 2015). This small difference is likely a combined result of (1) constant black carbon (BC) emissions in the Plio-Pristine and Plio-Polluted, whereas BC increases from PI to present day and contributes to a small positive ERF (Myhre et al., 2013), and (2) potentially nonlinear cloud responses to aerosol changes under different climate states.

Table 1
Annual global and Arctic (70–90°N) Adjusted Effective Radiative Forcing (aERF) Due to the Absence of Tropospheric Industrial Pollutants From Plio-Pristine. F_{dir}: Direct Radiative Forcing; F_{ACI}: Radiative Forcing Due to Aerosol Cloud Interactions

Region	aERF	F_{dir}	F_{ACI}
Global (annual)	1.29	0.18	1.11
Arctic (annual)	0.75	0.05	0.7

Note. Effective radiative forcing is adjusted to exclude the influence from surface albedo changes between experiments (see Text S2 for more details).

3.2. Energy Balance Analysis Results

We decompose simulated annual mean temperature changes between the Plio-Pristine and Plio-Polluted simulations (ΔT_s) linearly into contributions from changes in clear-sky and cloudy-sky planetary emissivity; changes in planetary albedo from changes in clear sky, cloudy sky (i.e., overcast), and surface reflection; and finally, changes in meridional heat convergence using a one-dimensional energy balance model. This analysis is adapted from previous publications (Heinemann et al., 2009; Hill et al., 2014; Lunt et al., 2012) by Feng et al. (2017) to incorporate

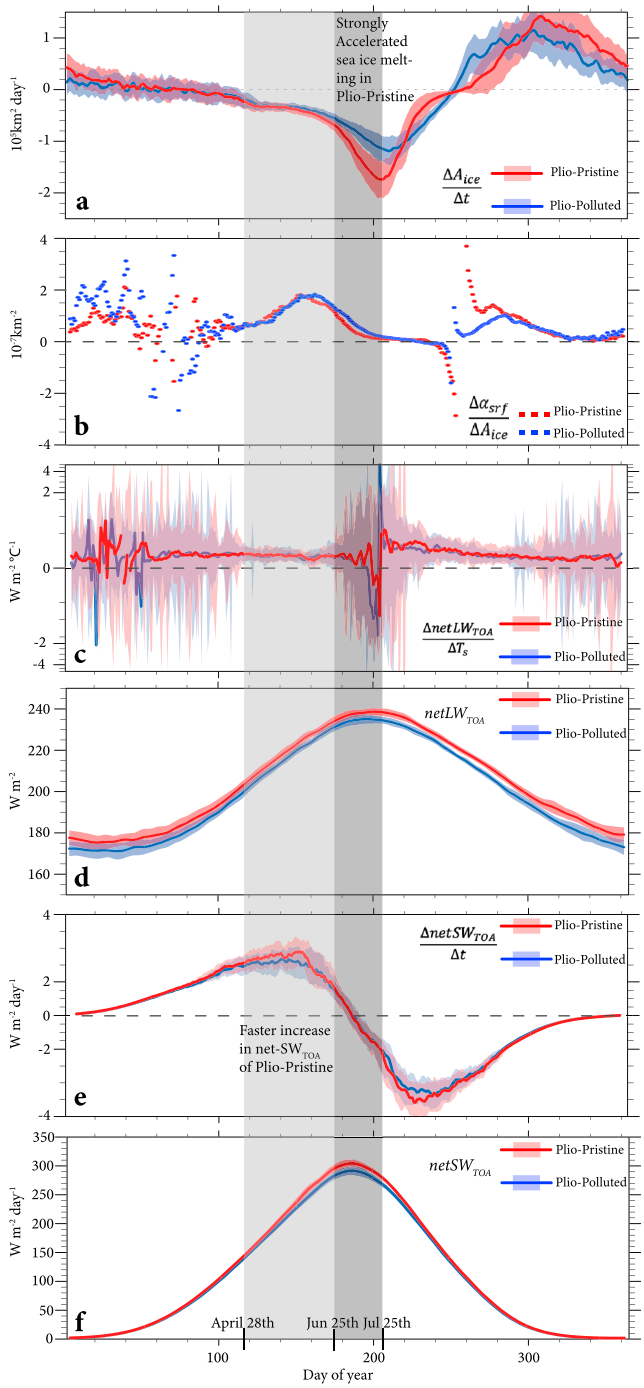

Figure 2. Feedback strengths and daily evolution of sea ice extent and radiation fluxes. (a and e) Daily rates of change of Arctic sea ice cover ($\frac{\Delta A_{ice}}{\Delta t}$), and net top of the atmosphere (TOA) shortwave absorption ($\frac{\Delta \text{netSW}_{TOA}}{\Delta t}$). The rate of change is calculated by subtracting values of previous day from current day. (b and c) Rates of surface albedo change as a function of sea ice cover change ($\frac{\Delta \alpha_{srf}}{\Delta A_{ice}}$), and rates of changes of net planetary longwave emission as a function of surface temperature change ($\frac{\Delta \text{netLW}_{TOA}}{\Delta T_s}$). (d and f) Daily climatology of net planetary longwave emission (netLW$_{TOA}$), and net planetary shortwave absorption (netSW$_{TOA}$). Shading shows one standard deviation from daily mean of 50 model years.

the approximate partial radiative perturbation method in order to better separate planetary albedo changes (Figure 1b). South of 60°N, surface warming in Plio-Pristine is primarily attributable to the reduction in cloudy-sky reflection (cld-α) and is partially offset by reduction in meridional heat convergence (H) and reduction in cloudy-sky greenhouse effect (cld-ε). These changes reflect the overall reduction in cloud amount as well as a slowing down of Atlantic Overturning Circulation (AMOC). Plio-Pristine features a mean freshening of the North Atlantic by 0.13 psu between 55 and 70°N and slowing down of the AMOC by 1.7 Sverdrup (Sv), measured by the maximum of the meridional stream function north of 30°N and below 500 m within the Atlantic Ocean basin. This ocean dynamical response leads to a reduction in northward ocean heat transport by 0.1 PW across 45°N, causing persistent cooling from changes in ocean heat convergence north of 45°N (Figure S3). Yet an increase in atmospheric heat transport mostly compensates this change (Figure S3). The AMOC in our simulations is in quasi-equilibrium state with small trends of 3×10^{-3} and 1×10^{-3} Sv/century for Plio-Pristine and Plio-Polluted. Yet thousands of years' model integration may show more diversity in AMOC behavior (Burls et al., 2017).

North of 60°N, surface warming is mostly driven by a reduction in surface reflection (srf-α), followed by a small contribution from reduction in clear-sky planetary emissivity (clr-ε). A small amount of this high-latitude warming is offset by an increase in cloud cover, causing an increase in cloud reflection. Increase in cloud reflection, however, is partially attenuated by an increase in cloudy-sky greenhouse effect (cld-ε). Contributions from heat convergence to surface warming vary between latitudes. Yet when integrated between 60°N and 90°N, the net contribution of meridional heat transport to the mean warming is negligible.

3.3. Key forcing and Feedback Contributing to September Sea Ice-Free Arctic Ocean

Plio-Pristine and Plio-Polluted simulate two stable Arctic Ocean states: seasonal sea ice and perennial sea ice (Eisenman & Wettlaufer, 2009) with only a 0.75 W/m^2 difference in net top of the atmosphere (TOA) radiative forcing. In order to explore feedbacks leading to these two Arctic Ocean states, we calculate mean strengths of various feedbacks and evolutions of radiative fluxes north of 60°N using daily model outputs of the final 50 years. The choice of 60°N is based on our EBA results that north of 60°N; the net effect of meridional heat transport to annual surface warming is negligible. This result also holds at seasonal time scale (Figure S4), which allows us to focus on radiation fluxes.

Planetary longwave feedback to surface temperature change ($\frac{\Delta \text{netLW}_{TOA}}{\Delta T_s}$; Figure 2c) and surface albedo response to sea ice cover change ($\frac{\Delta \alpha_{srf}}{\Delta A_{ice}}$) show strong interannual and daily variability, especially during the Arctic summer and winter when sea ice retreats and expands (Figure 2b). Yet the overlapping and similarity of calculated $\frac{\Delta \text{netLW}_{TOA}}{\Delta T_s}$ and $\frac{\Delta \alpha_{srf}}{\Delta A_{ice}}$ between experiments suggests that the strengths of longwave feedback and sea ice surface albedo feedback are similar between Plio-Pristine and Plio-Polluted. Major difference between two experiments occurs in the daily rate of net TOA shortwave absorption ($\frac{\Delta \text{netSW}_{TOA}}{\Delta t}$). Plio-Pristine features faster increase in net TOA shortwave absorption from May to June

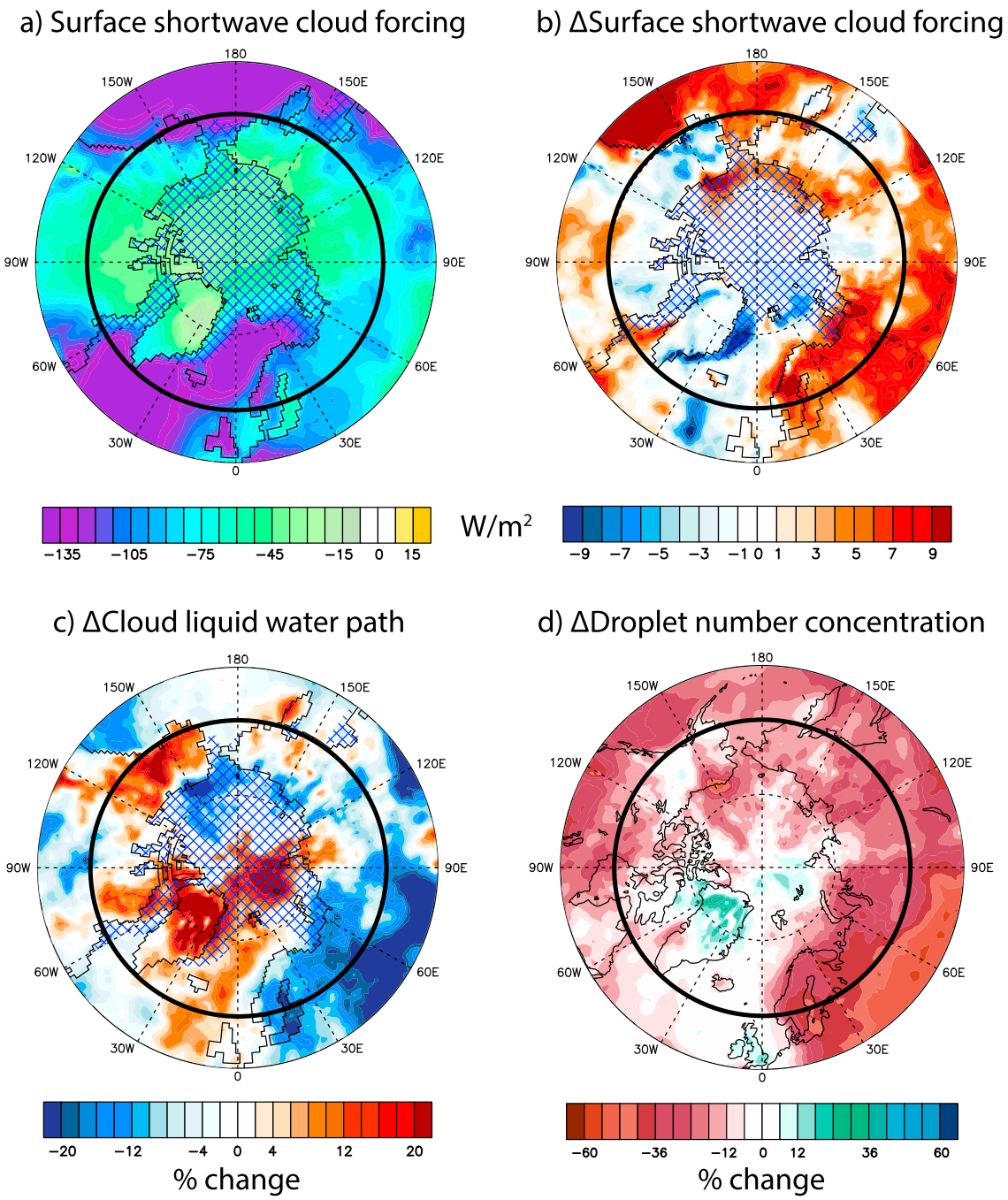

Figure 3. May to June average of (a) climatology of Plio-Polluted and (b) difference in surface shortwave cloud forcing, and percent difference in optical properties of clouds of Plio-Pristine minus Plio-Polluted. Optical properties include (c) cloud liquid water path, and (d) cloud droplet number concentration integrated through the whole troposphere column. Bold solid line highlights the 60°N. Blue hatches show climatology of sea ice cover in Plio-Pristine.

(Figures 2e and 2f). This enhanced shortwave absorption accelerates sea ice loss in Plio-Pristine, which predates the major melting phase occurring in July (Figures 1a and 2a).

The enhanced TOA shortwave absorption in Plio-Pristine can be explained by the attenuation of surface shortwave cloud forcing across the northern Europe and North Pacific (Figures 3a and 3b), measured by subtracting downwelling surface shortwave radiation of clear-sky condition from the full condition to reduce the contamination from ice masking (Hill et al., 2014). Shortwave cloud forcing is dependent on cloud

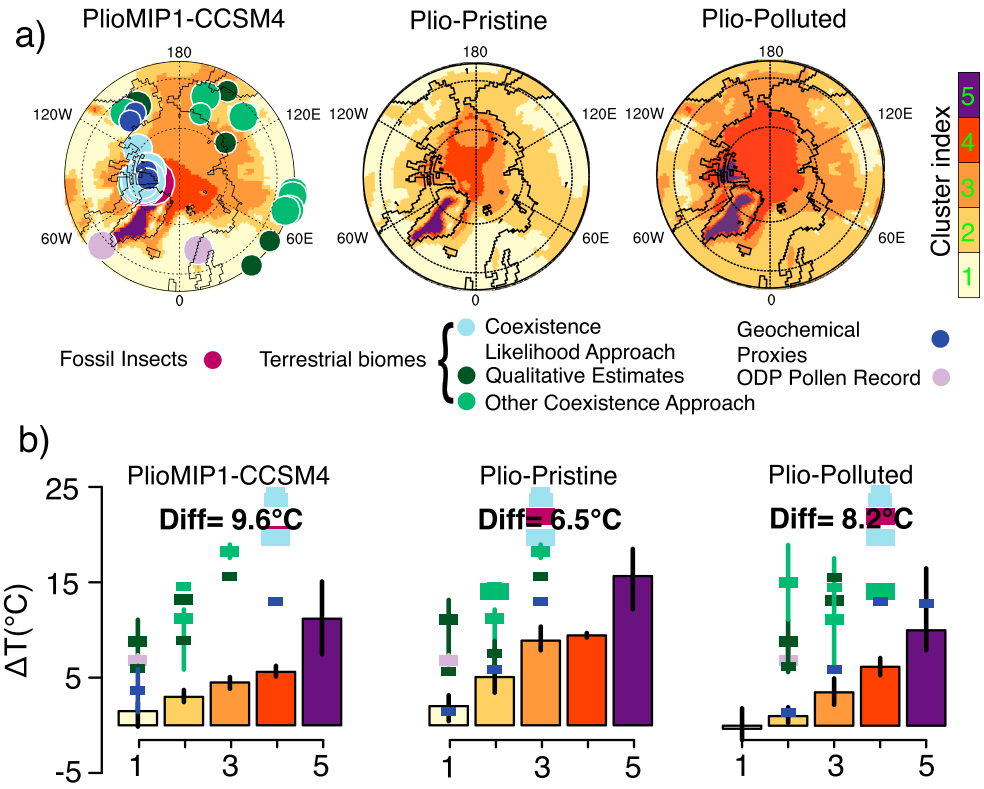

Figure 4. Cluster patterns and medians of the model simulated and proxy estimated northern high latitude (>55°N) surface warmth of mid-Piacenzian Warm period relative to preindustrial (ΔT). (a) Patterns of simulated warmth by PlioMIP1-CCSM4 (Rosenbloom et al., 2013), Plio-Pristine, and Plio-Polluted. In (a), bubbles show locations of proxy records. Bubble sizes scale with confidence levels of the records (Feng et al., 2017). Colors show reconstruction method and proxy source materials. (b) Medians of ΔT-model (bars) and ΔT-proxy (markers; ΔT-proxy = terrestrial proxy temperature − mean surface temperature of 1901–1930, Willmott, 2000). A vertical line on top of each bar spans the 5th and 95th percentiles of ΔT-model within each cluster. A vertical bar of ΔT-proxy shows the maximum and minimum of ΔT-proxy from the same proxy system. The calculated mean differences (Diff) between ΔT-proxy and ΔT-model based on cluster medians are also shown in (b).

optical depth (τ). The relative change in cloud optical depth of liquid clouds positively scales with the relative change in cloud liquid water content (LWC) and negatively scales with the relative change in droplet effective radius. The latter negatively scales with the relative change of droplet number concentration (N_c), and hence, $\frac{\Delta\tau}{\tau} \propto \left(\frac{\Delta \mathrm{LWC}}{\mathrm{LWC}}, \frac{\Delta N_c}{N_c}\right)$. This scaling is applicable to cloud ice crystals. The results are quite similar to the results of cloud droplets (Figure S5). Thereby, we focus on cloud droplets here. In Plio-Pristine, the attenuation of surface shortwave cloud forcing shows good correspondence with the reduction of cloud liquid water path across the northern Europe (Figure 3c) and reduction of cloud droplet number concentration in both north Pacific and northern Europe (Figure 3d), suggesting a shorter cloud life (second indirect effect) and lower cloud albedo (first indirect effect) due to the removal of pollutants.

Sea ice melting in Plio-Pristine is even more accelerated during July compared to Plio-Polluted, yet the evolution and sensitivity of radiation fluxes to sea ice loss are quite similar between two experiments (Figure 2). This accelerated melting, hence, is self-sustaining, and largely reflects the seasonally runaway ice-albedo feedback (Figure 1a). Sea ice loss slows down in the Plio-Pristine simulation during August due to increasing amount of longwave loss from the open ocean (Figure 2d), and there is a southward shift of the hemispheric insolation maxima (Figure 2f). Yet these radiation changes are insufficient to reverse the net sea ice loss trend, allowing Plio-Pristine to reach September sea ice-free Arctic Ocean.

During the late fall, low sea ice extent and a warmer Arctic ocean in Plio-Pristine initially slow down the sea ice expansion (Figure 2a). Yet ice expands quickly during the winter due to greater heat loss from the open ocean (Figure 2d; Eisenman & Wettlaufer, 2009). By the early spring, Arctic sea ice extent in Plio-Pristine reaches an annual maxima similar to Plio-Polluted, sustaining a stable seasonal Arctic sea ice state.

3.4. Comparison With Proxy Records

Strongly amplified Northern high latitude warmth during the MPWP is well known from terrestrial records north of 55°N (Fletcher et al., 2017; Salzmann et al., 2013) and relatively insensitive to Arctic Ocean gateway changes (Feng et al., 2017). We compare mean annual surface temperatures from terrestrial proxies with our model simulations north of 55°N based on cluster medians estimated separately from proxy and model data (Figure 4). Cluster patterns are derived from annual surface temperature differences between individual MPWP experiments and preindustrial experiments using the same version of the model (Figure 4a). The proxy cluster median for each cluster is calculated using records geographically located within the same cluster. The cluster analysis is conducted using Gaussian mixture model with five clusters determined by maximizing Bayesian information criterion and minimizing the number of clusters. This analysis is carried out with R "mclust" package (Scrucca et al., 2016). Details of the method are outlined in the previous study (Feng et al., 2017; Figure 4)

The Plio-Pristine simulation shows a large improvement in matching proxy records by an average of 3.1 °C in addition to the warming simulated by PlioMIP1-CCSM4 simulation. The latter shows a 9.6 °C gap between proxy and model with the simulation being too cold. Comparing Plio-Pristine with Plio-Polluted, 1.7 °C difference comes from elimination of pollutants, which may explain some of the differences of northern high latitude warmth between MPWP and present day.

4. Discussions and Conclusions

In our experiments, a small forcing induced by industrial pollutants is key to determining whether or not CESM1.2 enters the seasonally Arctic ice-free state of MPWP. This result suggests a nonlinear responses of Pliocene Arctic sea ice to perturbations. As shown by the previous study (Eisenman & Wettlaufer, 2009), the transition from a perennial to seasonal Arctic sea ice state as a function of increasing radiative forcing does not demonstrate hysteresis, yet the evolution is nonlinear. This behavior is supported by our atmosphere-ocean coupled simulations. It may contribute to explain the discontinuity in estimated global mean temperature response to CO_2 forcing between the Quaternary and Pliocene (Köhler et al., 2015). Nonlinear sea ice responses are also shown to occur in response to orbital forcing changes (e.g., Tabor et al., 2015).

Although our simulations highlight the importance of not including industrial pollutants and the associated aerosol indirect effects in paleoclimate simulations, pollutants are unlikely key to explaining the sea ice transition at the end of Pliocene (2.6 Ma; Knies et al., 2014). Perturbations to the MPWP Arctic radiation budget from changes in tropospheric dust loading (Sagoo & Storelvmo, 2017) and biogenic and forest fire emissions (Unger & Yue, 2014) may be plausible triggers in addition to declining CO_2.

Compared to Quaternary, MPWP likely has a lower atmospheric dust loading (Sagoo & Storelvmo, 2017), and enhanced emissions of greenhouse gases and particle precursors from vegetation and forest fire (Unger & Yue, 2014) due to its warm, moist, and more vegetated environment. Dust can promote cloud ice over cloud liquid formation (Shi & Liu, 2019) or a pure increase of cloud ice crystals (Sagoo & Storelvmo, 2017) in the mixed phase clouds. The dominancy of either effect can lead to a net warming (Shi & Liu, 2019) or cooling effect (Sagoo & Storelvmo, 2017) in response to increasing dust emission. With warm, moist, and forested Northern high latitudes, the emission and formation of greenhouse gases of methane, tropospheric ozone, and nitrous oxide are expected to increase (Unger & Yue, 2014), yet the enhanced biogenic emissions of aerosol precursors and emergence of frequent boreal forest fire (Fletcher et al., 2019) may create a constant flux of aerosols into the troposphere and hence promote cloud formation, and reflection of sunlight (Tunved et al., 2006). The net effect of these biogeochemical feedbacks is unknown and remains one of the most uncertain aspects of simulating past and future climate change at high latitudes.

On the other hand, different strengths of simulated Arctic feedbacks among models (Cronin et al., 2017; Goosse et al., 2018) also play a key role in determining the amount of forcings responsible for the rapid transition of Arctic sea ice state between perennial to seasonal. Our results indicate that the uncertainty of simulating this nonlinear behavior of sea ice may explain the diverse predictions of future Arctic Sea ice (Jahn et al., 2016; Stroeve et al., 2007; Stroeve et al., 2012).

Finally, the global mean temperature simulated in our mid-Piacenzian experiment free of tropospheric pollutants (i.e., Plio-Pristine) is 2.3 °C warmer than the preindustrial, and well within the proxy-estimated range for MPWP (Haywood & Valdes, 2004; Masson-Delmotte et al., 2013). This result is qualitatively consistent with recent findings suggesting high risk for seasonally sea ice-free Arctic with 2 °C global mean surface warming (Jahn, 2018; Sanderson et al., 2017). While current efforts to reduce industrial pollutants are no doubt beneficial, these efforts may actually lead to accelerated Arctic sea ice loss, as we continue approaching the forcing threshold for seasonally sea ice-free Arctic Ocean. The potential influences on weather and climate through complex interactions with radiation and atmospheric circulation may have already been on the way (Xu et al., 2018).

Acknowledgments
We would like to thank Natalie Burl and an anonymous reviewer for their helpful suggestions to improve this manuscript and high-performance computing support from Cheyenne (https://doi.org/10.5065/D6RX99HX) and Yellowstone (ark:/85065/d7wd3xhc) provided by NCAR's Computational and Information Systems Laboratory, sponsored by the National Science Foundation. This material is based upon work supported by the National Center for Atmospheric Research, which is a major facility sponsored by the National Science Foundation under Cooperative Agreement 1852977. Additional funding was provided by NSF grant 1814029 to Ran Feng, 1418411 to Bette L. Otto-Bliesner, and 1418421 to Ashley Ballantyne. We also would like to thank Nan Rosenbloom at NCAR for providing PlioMIP1 boundary conditions. The simulation data are hosted at Cheyenne supercomputer with the path: /CCSM/csm/CESM-CAM4-PLIOCENE. Instructions and permissions to relevant experiments will be provided upon request to ran.feng@uconn.edu.

References

Andreae, M. O. (2007). Aerosols before pollution. *Science*, *315*(5808), 50–51. https://doi.org/10.1126/science.1136529

Ballantyne, A. P., Greenwood, D. R., Damsté, J. S. S., Csank, A. Z., Eberle, J. J., & Rybczynski, N. (2010). Significantly warmer Arctic surface temperatures during the Pliocene indicated by multiple independent proxies. *Geology*, *38*(7), 603–606. http://doi.org/10.1130/G30815.1

Burls, N. J., Fedorov, A. V., Sigman, D. M., Jaccard, S. L., Tiedemann, R., & Haug, G. H. (2017). Active Pacific meridional overturning circulation (PMOC) during the warm Pliocene. *Science Advances*, *3*(9), e1700156. https://doi.org/10.1126/sciadv.1700156

Chandler, M., Rind, D., & Thompson, R. (1994). Joint investigations of the middle Pliocene climate II: GISS GCM Northern Hemisphere results. *Global and Planetary Change*, *9*(3-4), 197–219. https://doi.org/10.1016/0921-8181(94)90016-7

Chandler, M. A., Sohl, L. E., Jonas, J. A., Dowsett, H. J., & Kelley, M. (2013). Simulations of the mid-Pliocene Warm Period using two versions of the NASA/GISS ModelE2-R Coupled Model. *Geoscientific Model Development*, *6*(2), 517–531. https://doi.org/10.5194/gmd-6-517-2013

Cronin, T. W., Li, H., & Tziperman, E. (2017). Suppression of Arctic air formation with climate warming: investigation with a two-dimensional cloud-resolving model. *Journal of the Atmospheric Sciences*, *74*(9), 2717–2736. https://doi.org/10.1175/JAS-D-16-0193.1

Csank, A. Z., Tripati, A. K., Patterson, W. P., Eagle, R. A., Rybczynski, N., Ballantyne, A. P., & Eiler, J. M. (2011). Estimates of Arctic land surface temperatures during the early Pliocene from two novel proxies. *Earth and Planetary Science Letters*, *304*(3-4), 291–299. https://doi.org/10.1016/j.epsl.2011.02.030

Dowsett, H., Dolan, A., Rowley, D., Moucha, R., Forte, A. M., Mitrovica, J. X., et al. (2016). The PRISM4 (mid-Piacenzian) paleoenvironmental reconstruction. *Climate of the Past*, *12*(7), 1519–1538. https://doi.org/10.5194/cp-12-1519-2016

Eisenman, I., & Wettlaufer, J. S. (2009). Nonlinear threshold behavior during the loss of Arctic sea ice. *Proceedings of the National Academy of Sciences*, *106*(1), 28–32. https://doi.org/10.1073/pnas.0806887106

Feng, R., Otto-Bliesner, B. L., Fletcher, T. L., Tabor, C. R., Ballantyne, A. P., & Brady, E. C. (2017). Amplified Late Pliocene terrestrial warmth in northern high latitudes from greater radiative forcing and closed Arctic Ocean gateways. *Earth and Planetary Science Letters*, *466*, 129–138. https://doi.org/10.1016/j.epsl.2017.03.006

Fletcher, T., Feng, R., Telka, A. M., Matthews, J. V. Jr., & Ballantyne, A. (2017). Floral Dissimilarity and the influence of climate in the Pliocene High Arctic: Biotic and abiotic influences on five sites on the Canadian Arctic Archipelago. *Frontiers in Ecology and Evolution*, *5*, 19.

Fletcher, T. L., Warden, L., Sinninghe Damsté, J. S., Brown, K. J., Rybczynski, N., Gosse, J. C., & Ballantyne, A. P. (2019). Evidence for fire in the Pliocene Arctic in response to amplified temperature. *Climate of the Past*, *15*(3), 1063–1081. https://doi.org/10.5194/cp-15-1063-2019

Gagné, M. È., Gillett, N. P., & Fyfe, J. C. (2015). Impact of aerosol emission controls on future Arctic sea ice cover. *Geophysical Research Letters*, *42*, 8481–8488. https://doi.org/10.1002/2015GL065504

Gettelman, A. (2015). Putting the clouds back in aerosol–cloud interactions. *Atmospheric Chemistry and Physics*, *15*(21), 12397–12411. https://doi.org/10.5194/acp-15-12397-2015

Gettelman, A., Liu, X., Ghan, S. J., Morrison, H., Park, S., Conley, A. J., et al. (2010). Global simulations of ice nucleation and ice supersaturation with an improved cloud scheme in the Community Atmosphere Model. *Journal of Geophysical Research*, *115*, D18216. https://doi.org/10.1029/2009JD013797

Gettelman, A., Shindell, D. T., & Lamarque, J.-F. (2015). Impact of aerosol radiative effects on 2000–2010 surface temperatures. *Climate Dynamics*, *45*(7-8), 2165–2179.

Ghan, S. J., Liu, X., Easter, R. C., Zaveri, R., Rasch, P. J., Yoon, J.-H., & Eaton, B. (2012). Toward a minimal representation of aerosols in climate models: Comparative decomposition of aerosol direct, semidirect, and indirect radiative forcing. *Journal of Climate*, *25*(19), 6461–6476. https://doi.org/10.1175/JCLI-D-11-00650.1

Goosse, H., Kay, J. E., Armour, K. C., Bodas-Salcedo, A., Chepfer, H., Docquier, D., et al. (2018). Quantifying climate feedbacks in polar regions. *Nature Communications*, *9*(1), 1919. https://doi.org/10.1038/s41467-018-04173-0

Haywood, A. M., Dowsett, H. J., & Dolan, A. M. (2016). Integrating geological archives and climate models for the mid-Pliocene warm period. *Nature Communications*, *7*(1). http://doi.org/10.1038/ncomms10646

Haywood, A. M., Dowsett, H. J., Otto-Bliesner, B., Chandler, M. A., Dolan, A. M., Hill, D. J., et al. (2010). Pliocene Model Intercomparison Project (PlioMIP): Experimental design and boundary conditions (Experiment 1). *Geoscientific Model Development*, *3*(1), 227–242. http://doi.org/10.5194/gmd-3-227-2010

Haywood, A. M., & Valdes, P. J. (2004). Modelling Pliocene warmth: contribution of atmosphere, oceans and cryosphere. *Earth and Planetary Science Letters*, *218*(3-4), 363–377. http://doi.org/10.1016/S0012-821X(03)00685-X

Heinemann, M., Jungclaus, J. H., & Marotzke, J. (2009). Warm Paleocene/Eocene climate as simulated in ECHAM5/MPI-OM. *Climate of the Past*, *5*(4), 785–802. https://doi.org/10.5194/cp-5-785-2009

Hill, D. J. (2015). The non-analogue nature of Pliocene temperature gradients. *Earth and Planetary Science Letters*, *425*, 232–241. https://doi.org/10.1016/j.epsl.2015.05.044

Hill, D. J., Haywood, A. M., Lunt, D. J., Hunter, S. J., Bragg, F. J., Contoux, C., et al. (2014). Evaluating the dominant components of warming in Pliocene climate simulations. *Climate of the Past*, *10*(1), 79–90. http://doi.org/10.5194/cp-10-79-2014

Howell, F. W., Haywood, A. M., Dowsett, H. J., & Pickering, S. J. (2016). Sensitivity of Pliocene Arctic climate to orbital forcing, atmospheric CO_2 and sea ice albedo parameterisation. *Earth and Planetary Science Letters*, *441*, 133–142. https://doi.org/10.1016/j.epsl.2016.02.036

Howell, F. W., Haywood, A. M., Otto-Bliesner, B. L., Chandler, M. A., & Rosenbloom, N. A. (2016). Arctic sea ice simulation in the PlioMIP ensemble. *Climate of the Past*, *12*(3), 749–767. https://doi.org/10.5194/cp-12-749-2016

Hurrell, J. W., Hack, J. J., Shea, D., Caron, J. M., & Rosinski, J. (2008). A new sea surface temperature and sea ice boundary dataset for the Community Atmosphere Model. *Journal of Climate*, *21*(19), 5145–5153. https://doi.org/10.1175/2008JCLI2292.1

Hurrell, J. W., Holland, M. M., Gent, P. R., Ghan, S., Kay, J. E., Kushner, P. J., et al. (2013). The community earth system model: a framework for collaborative research. *Bulletin of the American Meteorological Society*, *94*(9), 1339–1360. https://doi.org/10.1175/BAMS-D-12-00121.1

Jahn, A. (2018). Reduced probability of ice-free summers for 1.5 °C compared to 2 °C warming. *Nature Climate Change*, *8*(5), 409.

Jahn, A., Kay, J. E., Holland, M. M., & Hall, D. M. (2016). How predictable is the timing of a summer ice-free Arctic? *Geophysical Research Letters*, *43*, 9113–9120. https://doi.org/10.1002/2016GL070067

Kay, J. E., Hillman, B. R., Klein, S. A., Zhang, Y., Medeiros, B., Pincus, R., et al. (2012). Exposing global cloud biases in the Community Atmosphere Model (CAM) using satellite observations and their corresponding instrument simulators. *Journal of Climate*, *25*(15), 5190–5207. https://doi.org/10.1175/JCLI-D-11-00469.1

Kiehl, J. T., & Shields, C. A. (2013). Sensitivity of the Palaeocene-Eocene Thermal Maximum climate to cloud properties. *Philosophical Transactions of the Royal Society of London a: Mathematical, Physical and Engineering Sciences*, *371*(2001), 20130093. http://doi.org/10.1098/rsta.2013.0093

Knies, J., Cabedo-Sanz, P., Belt, S. T., Baranwal, S., Fietz, S., & Rosell-Melé, A. (2014). The emergence of modern sea ice cover in the Arctic Ocean. *Nature Communications*, *5*(1), 5608. http://doi.org/10.1038/ncomms6608

Köhler, P., de Boer, B., von der Heydt, A. S., Stap, L. B., & van de Wal, R. S. (2015). On the state-dependency of the equilibrium climate sensitivity during the last 5 million years. *Climate of the Past*, *11*(12), 1801–1823. https://doi.org/10.5194/cp-11-1801-2015

Kump, L. R., & Pollard, D. (2008). Amplification of Cretaceous warmth by biological cloud feedbacks. *Science*, *320*(5873), 195–195. http://doi.org/10.1126/science.1153883

Lamarque, J. F., Bond, T. C., Eyring, V., Granier, C., Heil, A., Klimont, Z., et al. (2010). Historical (1850–2000) gridded anthropogenic and biomass burning emissions of reactive gases and aerosols: methodology and application. *Atmospheric Chemistry and Physics*, *10*(15), 7017–7039. https://doi.org/10.5194/acp-10-7017-2010

Lisiecki, L. E., & Raymo, M. E. (2005). A Pliocene-Pleistocene stack of 57 globally distributed benthic $\delta^{18}O$ records. *Paleoceanography*, *20*, PA1003. https://doi.org/10.1029/2004PA001071

Lunt, D. J., Haywood, A. M., Schmidt, G. A., Salzmann, U., Valdes, P. J., Dowsett, H. J., & Loptson, C. A. (2012). On the causes of mid-Pliocene warmth and polar amplification. *Earth and Planetary Science Letters*, *321-322*, 128–138. http://doi.org/10.1016/j.epsl.2011.12.042

Masson-Delmotte, V., Schulz, M., Abe-Ouchi, A., Beer, J., Ganopolski, A., González Rouco, J. F., et al. (2013). Information from paleoclimate archives. *Climate Change*, 383464.

Meehl, G. A., Washington, W. M., Arblaster, J. M., Hu, A., Teng, H., Kay, J. E., et al. (2013). Climate change projections in CESM1(CAM5) compared to CCSM4. *Journal of Climate*, *26*(17), 6287–6308. http://doi.org/10.1175/JCLI-D-12-00572.1

Myhre, G., Shindell, D., Bréon, F. M., Collins, W., Fuglestvedt, J., Huang, J., et al. (2013). Anthropogenic and natural radiative forcing. *Climate Change*, *423*, 658–740.

Naafs, B. D. A., Stein, R., Hefter, J., Khélifi, N., de Schepper, S., & Haug, G. H. (2010). Late Pliocene changes in the North Atlantic current. *Earth and Planetary Science Letters*, *298*(3-4), 434–442. https://doi.org/10.1016/j.epsl.2010.08.023

Navarro, J. A., Varma, V., Riipinen, I., Seland, Ø., Kirkevåg, A., Struthers, H., et al. (2016). Amplification of Arctic warming by past air pollution reductions in Europe. *Nature Geoscience*, *9*(4), 277–281. https://doi.org/10.1038/ngeo2673

Neale, R. B., Gettelman, A., Park, S., Conley, A. J., Kinnison, D., Marsh, D., et al. (2010). Description of the NCAR community atmosphere model (CAM 5.0). *NCAR Tech. Note NCAR/TN-486+ STR*, *1*(1), 1–12.

Neale, R. B., Richter, J. H., Conley, A. J., Park, S., Lauritzen, P. H., Gettelman, A., et al. (2010). Description of the NCAR Community Atmosphere Model (CAM 4.0).

Otto-Bliesner, B. L., Jahn, A., Feng, R., Brady, E. C., Hu, A., & Löfverström, M. (2017). Amplified North Atlantic warming in the late Pliocene by changes in Arctic gateways. *Geophysical Research Letters*, *44*, 957–964. https://doi.org/10.1002/2016GL071805

Polyak, L., Alley, R. B., Andrews, J. T., Brigham-Grette, J., Cronin, T. M., Darby, D. A., et al. (2010). History of sea ice in the Arctic. *Quaternary Science Reviews*, *29*(15-16), 1757–1778. https://doi.org/10.1016/j.quascirev.2010.02.010

Prescott, C. L., Haywood, A. M., Dolan, A. M., Hunter, S. J., Pope, J. O., & Pickering, S. J. (2014). Assessing orbitally-forced interglacial climate variability during the mid-Pliocene Warm Period. *Earth and Planetary Science Letters*, *400*, 261–271. https://doi.org/10.1016/j.epsl.2014.05.030

Robinson, M. M., Valdes, P. J., & Haywood, A. M. (2011). Bathymetric controls on Pliocene North Atlantic and Arctic sea surface temperature and deepwater production. *Palaeogeography, Palaeoclimatology, Palaeoecology*, *309*(1-2), 92–97. https://doi.org/10.1016/j.palaeo.2011.01.004

Rosenbloom, N. A., Otto-Bliesner, B. L., Brady, E. C., & Lawrence, P. J. (2013). Simulating the mid-Pliocene Warm Period with the CCSM4 model. *Geoscientific Model Development*, *6*(2), 549–561. http://doi.org/10.5194/gmd-6-549-2013

Rybczynski, N., Gosse, J. C., Harington, C. R., Wogelius, R. A., Hidy, A. J., & Buckley, M. (2013). Mid-Pliocene warm-period deposits in the High Arctic yield insight into camel evolution. *Nature Communications*, *4*(1), 1550. https://doi.org/10.1038/ncomms2516

Sagoo, N., & Storelvmo, T. (2017). Testing the sensitivity of past climates to the indirect effects of dust. *Geophysical Research Letters*, *44*, 5807–5817. https://doi.org/10.1002/2017GL072584

Salzmann, U., Dolan, A. M., Haywood, A. M., Chan, W.-L., Voss, J., Hill, D. J., et al. (2013). Challenges in quantifying Pliocene terrestrial warming revealed by data–model discord. *Nature Climate Change*, *3*(11), 969–974. https://doi.org/10.1038/nclimate2008

Sanderson, B. M., Xu, Y., Tebaldi, C., Wehner, M., O'Neill, B., Jahn, A., et al. (2017). Community climate simulations to assess avoided impacts in 1.5 and 2 ° C futures. *Earth System Dynamics*, *8*(3), 827–847. https://doi.org/10.5194/esd-8-827-2017

Scrucca, L., Fop, M., Murphy, T. B., & Raftery, A. E. (2016). mclust 5: clustering, classification and density estimation using Gaussian finite mixture models. *The R Journal*, *8*(1), 289.

Shi, Y., & Liu, X. (2019). Dust radiative effects on climate by glaciating mixed-phase clouds. *Geophysical Research Letters*, *46*, 6128–6137. https://doi.org/10.1029/2019GL082504

Smith, R. (1990). A scheme for predicting layer clouds and their water content in a general circulation model. *Quarterly Journal of the Royal Meteorological Society*, *116*(492), 435–460. https://doi.org/10.1002/qj.49711649210

Solomon, S., Plattner, G.-K., Knutti, R., & Friedlingstein, P. (2009). Irreversible climate change due to carbon dioxide emissions. *Proceedings of the National Academy of Sciences*, *106*(6), 1704–1709. https://doi.org/10.1073/pnas.0812721106

Stroeve, J., Holland, M. M., Meier, W., Scambos, T., & Serreze, M. (2007). Arctic sea ice decline: Faster than forecast. *Geophysical Research Letters*, *34*, L09501. https://doi.org/10.1029/2007GL029703

Stroeve, J. C., Kattsov, V., Barrett, A., Serreze, M., Pavlova, T., Holland, M., & Meier, W. N. (2012). Trends in Arctic sea ice extent from CMIP5, CMIP3 and observations. *Geophysical Research Letters*, *39*, L16502. https://doi.org/10.1029/2012GL052676

Tabor, C. R., Poulsen, C. J., & Pollard, D. (2015). How obliquity cycles powered early Pleistocene global ice-volume variability. *Geophysical Research Letters*, *42*, 1871–1879. https://doi.org/10.1002/2015GL063322

Tunved, P., Hansson, H.-C., Kerminen, V.-M., Ström, J., Dal Maso, M., Lihavainen, H., et al. (2006). High natural aerosol loading over boreal forests. *Science*, *312*(5771), 261–263. https://doi.org/10.1126/science.1123052

Unger, N., & Yue, X. (2014). Strong chemistry-climate feedbacks in the Pliocene. *Geophysical Research Letters*, *41*, 527–533. http://doi.org/10.1002/2013GL058773

Willmott, C. J. (2000). Terrestrial air temperature and precipitation: Monthly and annual time series (1950-1996). *WWW Url: Http:// Climate. Geog. Udel. Edu/~ Climate/Html_Pages/README. Ghcn_Ts Html*.

Xu, Y., Lamarque, J.-F., & Sanderson, B. M. (2018). The importance of aerosol scenarios in projections of future heat extremes. *Climatic Change*, *146*(3-4), 393–406.

Zheng, J., Zhang, Q., Li, Q., Zhang, Q., & Cai, M. (2019). Contribution of sea ice albedo and insulation effects to Arctic amplification in the EC-Earth Pliocene simulation. *Climate of the Past*, *15*(1), 291–305. https://doi.org/10.5194/cp-15-291-2019